Analytica Chimica Acta 1135 (2020) 132–141

Contents lists available at ScienceDirect

Analytica Chimica Acta

journal homepage: www.elsevier.com/locate/aca

Determination of hydrogen peroxide released from cancer cells by a Fe-Organic framework/horseradish peroxidase-modified electrode

Tian Jiang , Xiuxiu Sun , Lingli Wei , Maoguo Li *

Anhui Key Laboratory of Chemo-Biosensing, College of Chemistry and Materials Science, Anhui Normal University, Wuhu, 241000, PR China

HIGHLIGHTS

- Untreated multi-walled carbon nanotubes were used as conductive carrier to accelerate the electron transfer of HRP.
- The addition of NH_2-MIL-53(Fe) had a good synergistic effect on the electron transfer of HRP.
- Drying temperature of the electrode had a great influence on the peak current.
- The stability of NH_2-MIL-53(Fe) and HRP was studied by SEM, XRD and UV–vis methods.
- This work developed a new platform for direct detection of H_2O_2 released from Hela and HepG2 cells.

GRAPHICAL ABSTRACT

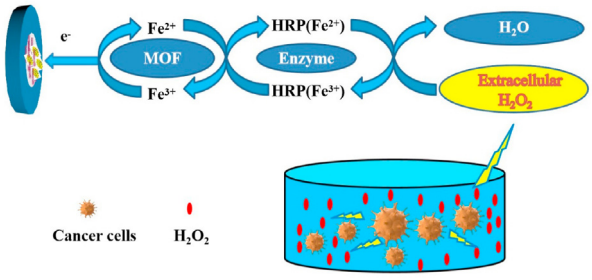

ARTICLE INFO

Article history:
Received 23 July 2020
Received in revised form
16 September 2020
Accepted 23 September 2020
Available online 25 September 2020

Keywords:
Hydrogen peroxide
Cancer cells
Metal organic framework
Horseradish peroxidase
Biosensors

ABSTRACT

Multi-walled carbon nanotubes (MWCNTs) were used as conductive carrier on the glassy carbon electrode (GCE), and the hybrid of metal organic framework [NH_2-MIL-53(Fe)] and horseradish peroxidase (HRP) was prepared by simple physical mechanical mixture. The GCE modified by the above material with immobilization, namely NH_2-MIL-53(Fe)/HRP/MWCNTs/GCE, was used to construct an electrochemical biosensor toward H_2O_2. The results indicated that the addition of NH_2-MIL-53(Fe) had a good synergistic effect on the electron transfer of HRP and the detection of H_2O_2. Under the optimized condition, the biosensor exhibited excellent electrochemical performances such as low detection limit, high sensitivity, good stability and so on. The H_2O_2 biosensor showed two linear ranges of 0.1–1 μM and 1–600 μM with a calculated detection limit of 0.028 μM (signal-to-noise ratio, S/N = 3). In addition, the stability of the hybrid of NH_2-MIL-53(Fe) and HRP were discussed by SEM, XRD and UV–vis methods. Furthermore, the reported biosensors were practically used in direct detection of H_2O_2 released from HeLa and HepG2 cells successfully. Thus, this work provides a new strategy to fabricate electrochemical biosensors using MOFs and biomolecules.

1. Introduction

Hydrogen peroxide (H_2O_2), a kind of typical reactive oxygen species (ROS) and strong oxidant, has certain physiological functions. For instance, H_2O_2 in granulocytes and phagocytes can oxidate

* Corresponding author.
E-mail address: limaoguo@mail.ahnu.edu.cn (M. Li).

https://doi.org/10.1016/j.aca.2020.09.040
0003-2670/

and kill the invading bacteria [1,2]. However, if the concentration of H_2O_2 is beyond the physical scope of cells, human body may be harmed because of excessive oxidative stress and damage to cells [1,3]. Therefore, the human body contains a variety of antioxidant enzymes, small molecule antioxidants and other antioxidants, which form a significant defense system to combat the side effects of ROS [4]. H_2O_2, as a by-product of various enzymatic reactions in the process of oxidative metabolism, is an important cellular metabolite and a biological/disease marker, playing a crucial role in the medical field [5,6]. Cancer cells have an altered mitochondrial redox state, typically characterized by the high levels of ROS such as H_2O_2 [7], it is of great significance to develop a platform that can be directly used for the determination of H_2O_2 released from cancer cells.

The common methods for detecting H_2O_2 include titrimetry [8], colorimetry [9], fluorescence [10,11], chemiluminescence [12], electrochemical luminescence [13], electrochemical sensing [14–16], photoelectrochemical sensing [17] and so on. Among these methods mentioned above, some method operation is simple but only for macro analysis, some method detection limit is low but sensitivity is not enough, some method with high sensitivity but has poor selectivity or instrument is expensive and so on. Electrochemical sensors have attracted the interest of many researchers due to their advantages such as low cost, simple operation and quick reaction. Meanwhile, some electrochemical sensors can be designed as portable devices. Therefore, it is a good choice to construct an electrochemical sensor for the determination of H_2O_2 released from cancer cells.

H_2O_2 electrochemical sensors can generally be divided into two categories: involving enzymes and non-enzymes. The electrochemical sensors involving enzymes are used by researchers quickly because this kind of sensors are based on biological recognition for high selectivity and possess electrochemical transduction process for good sensitivity [5]. Enzymes, known as proteins, usually have large and complex structure, where the redox centers are deeply immersed in the bodies, and three-dimensional structures hinder interaction with the electrode, the adsorptive denaturation of proteins onto electrodes and the unfavorable orientations at the electrode. However, the successful preparation of enzymes-based biosensors with direct electron transfer without electronic media will provide higher selectivity. And there will be less interference reactions because they can operate in a potential window closer to the redox potential of the enzymes [18].

Horseradish peroxidase (HRP) is an ideal substance to research direct electron transfer of enzymes. Non-electronic media of peroxidase-based sensors for low concentration H_2O_2 lack enough sensitivity, because the direct electron transfer process between the common electrode materials and peroxidase is slower [19]. To accelerate electron transfer between the enzyme and the electrode surface, materials with excellent conductivity can introduced such as multi-walled carbon nanotubes (MWCNTs). MWCNTs characterize high conductivity, chemical stability, large surface area and high mechanical strength which have been widely used in electrochemical biosensors. In MWCNTs, each CNT can act as a nano-electrode that facilitates the electron transfer without any mediators [20]. MWCNTs have previously been reported in relevant literature for accelerating electron transfer between HRP and the electrode surface [21,22].

Based on the realization of promoting electron transfer between HRP and the electrode surface, in order to further improve the electrochemical catalytic activity of the sensor and reduce the cost, we can introduce peroxidase-like nanometer materials. It's no doubt that metal organic frameworks (MOFs) are good introduction objects, because MOFs generally have large specific surface area, tunable porosity, uniform distribution of the metal centers and so on [23]. Many literatures have reported some peroxidase-like MOFs, such as Fe-MOF [23,24], Co-MOF [25,26], Ni-MOF [27,28], Cu-MOF [29–31], Zr-MOF [32]. Because HRP has Fe(III)/Fe (II) active center, we will prefer to choose the MOFs with iron metal center. Up to now, only limited Fe(III)-based MOFs, namely Fe-MIL-88NH_2, PCN-222(Fe) with porphyrinic Fe(III) centers, MIL-53(Fe), MIL-68(Fe) and MIL-100(Fe) were reported to exhibit intrinsic peroxidase-like catalytic activity [23]. MIL-53(M) is a kind of typical MOFs series, with the flexible structure, stable chemical properties and stable breathing characteristics, etc. In addition, the high-valence metal ion Fe^{3+} center and the most used carboxylate-type ligands can be easily used to synthesize water stable MOFs [33]. In order to make the MOFs and HRP mixed more evenly in the water solution, introducing hydrophilic functional groups such as $-NH_2$ to the ligands of MIL-53(Fe) can synthesize amino functional MIL-53(Fe), namely NH_2-MIL-53(Fe).

In this work, an electrochemical H_2O_2 biosensor has been designed simply by first modifying a layer of MWCNTs as a conductive substrate and carrier on the surface of glassy carbon electrode (GCE) for promoting the rate of electron transfer, then casting the mixture solution of NH_2-MIL-53(Fe) and HRP when the DMF solution of MWCNTs was semi-dry. Finally, the NH_2-MIL-53(Fe)/HRP/MWCNTs/GCE was prepared by fixing the above modified materials with Nafion. The results suggest that the introduction of NH_2-MIL-53(Fe) can achieve a good synergistic effect between Fe(III)/Fe(II) redox activity center of MOF and that of HRP. The optimization of experimental conditions was studied in detail. At the same time, the synergistic effect between NH_2-MIL-53(Fe) and HRP was also explored. The electrochemical biosensor under optimal conditions had good electro-catalytic and analytical properties for H_2O_2. And the biosensor could directly detect H_2O_2 released from HeLa and HepG2 cells, which had a practical application value.

2. Experimental

2.1. Preparation of NH_2-MIL-53(Fe)

The reagents and apparatus used in this work are listed in the supporting information (Tables S1 and S2). NH_2-MIL-53(Fe) was synthesized by reference to the method reported in literature [34] with some modifications. Firstly, 0.4040 g $Fe(NO_3)_3 \cdot 9H_2O$ (1 mmol), 0.1818 g 2-Aminoterephalic acid (H_2ATA, 1 mmol), 10 mL DMF were added into a Teflon autoclave (50 mL). Then the above solution was vigorously stirred at ambient temperature to reach transparency before thermal treatment at 150 °C for 6 h. When the autoclave and its container were cooled to room temperature, the as-synthesized particles were isolated by centrifugation with DMF and methanol each for at least three times successively until the supernatant liquid was clear. Finally, the samples were collected and vacuum treated at 60 °C for 12 h. The obtained powder is named as NH_2-MIL-53(Fe).

For comparison, we synthesized MIL-53(Fe) by replacing the ligand H_2ATA into terephthalic acid (H_2BDC) and keep the reaction temperature at 120 °C for 8 h according to the reported work [35]. The molar ratio of all the above reactants and other steps were the same as those in the preparation process of NH_2-MIL-53(Fe). The as-prepared sample is denoted as MIL-53(Fe).

2.2. Preparation of stock solutions

Firstly, 1 mg MWCNTs were dispersed in 1 mL DMF with ultrasonication (Power display, 100%) for 30 min. Subsequently, 1 mg HRP and 1 mg NH_2-MIL-53(Fe) were dispersed in 200 μL 0.1 M phosphate buffer solution (PBS, pH = 7.0) with ultrasonication (Power display, 40%) for 30 min and then shaking on the shaker at 1000 rpm for 1 h. For comparison, other stock solutions were prepared in the same manner as above, including 5 mg/mL HRP, 5 mg/mL NH_2-MIL-53(Fe) and 5 mg/mL MIL-53(Fe). In addition, 0.05 wt% Nafion stock solution was obtained by diluting the stoste which mass concentration is 5%. The solutions above were stored at 4 °C in the refrigerator.

2.3. Preparation of NH_2-MIL-53(Fe)/HRP/MWCNTs/GCE

2.3.1. Pre-treatment

Prior to use, the bare GCE was carefully polished with alumina powder (1.0, 0.3 and 0.05 μm in order) on wet chamois leather and then thoroughly cleaned ultrasonically in ethanol and water. All the as-prepared stock solutions were ultrasonic-treated for 10 min (Power display, 40%) every time before use.

2.3.2. Electrode modification

Firstly, 3 μL MWCNTs/DMF stock solution (1 mg/mL) was transferred to the surface of the GCE. Then when the MWCNTs/DMF was semi-dry at 37 °C in the air oven (about 10 min), the mixture of NH_2-MIL-53(Fe)/HRP stock solution (3 μL, 5 mg/mL) and 2 μL 0.05 wt% Nafion/water solution were added onto the surface of MWCNTs/GCE. Finally, the electrode was dried at 37 °C until the wet modified materials were totally dry. For comparison, other modified electrodes were prepared in a similar way.

2.4. Procedure for the electrochemical determination of H_2O_2

The NH_2-MIL-53(Fe)/HRP/MWCNTs/GCE was prepared as a working electrode and tested by.

Amperometric i-t Curve (i-t) technique, which was applied in −0.4 V vs. SCE from 0 to 100 s in 0.1 M PBS (pH = 7.0) until the signal was stable. Then, H_2O_2 solutions with different concentrations were added quantitatively to the blank buffer solution. After each sample addition, record the current response at 60 s when the current was stabilized again.

2.5. Cell culture

The complete medium was usually prepared by using RPMI 1640 medium to fix the volume to 50 mL at the present of 5 mL 10% fetal bovine serum (FBS) and 0.5 mL 1% penicillin-streptomycin. Human cervical carcinoma HeLa cells and human hepatoma HepG2 cells were grown in the aseptic culture flasks containing 4 mL complete medium. Then the culture flasks were placed at 37 °C in the incubator under an atmosphere containing 5% CO_2. Before the cells were passaged by trypsin digestion, the number of cells should be observed by the microscope. The cells could be sub-cultured when the number of cells was about 80%, the cell morphology is adherent growth at the moment. All the cell cultivation solutions that had been dumped during the sub-culture were collected, which were detected as real samples without any further treatment.

2.6. The investigation of the changing cell environment on H_2O_2 released from cells

Herein, we conducted two groups of HeLa or HepG2 cell culture, one was as the control group, which maintained normal cell culture process. Another was co-cultured with 100 μM ART (DMSO) after the normal culture for 24 h. Then the two above cell culture samples were continued to be cultured for another 24 h. We respectively collected the culture solutions and conducted electrochemical analysis toward H_2O_2 immediately.

3. Results and discussion

3.1. Characterization of the materials

Scanning electron microscopy (SEM) or Transmission electron microscope (TEM), X-ray power diffraction (XRD) and X-ray photoelectron spectroscopy (XPS) were used to characterize the morphology, crystal structure and valence state of the materials. Compare Fig. 1A with Fig. S1A, the main diffraction peaks of synthesized MOFs are consistent with those reported in the literature [34], which suggests that MIL-53(Fe) and NH_2-MIL-53(Fe) were successfully synthesized. In order to determine the groups in the MOFs, the Fourier transform infrared (FT-IR) analysis of MIL-53(Fe) and NH_2-MIL-53(Fe) was carried out. As shown in Fig. 1B, since the ligand of the two MOFs are terephthalic acid and its derivatives, it can be seen from the FT-IR spectra that both materials contain the infrared characteristic peaks of Ar-(*O*–*C*–O) (~1580 cm-1–1375 cm^{-1}), Ar *C*–H (~750 cm^{-1}), Ar *C*–C (~1500 cm^{-1}) and C=O (~1680 cm^{-1}) [34]. In addition, both spectra have the infrared characteristic peak of Fe–O bond near 560 cm^{-1}, but the infrared peak of Fe–O bond of MIL-53(Fe) is stronger and sharper. The difference between the infrared spectra of the two MOFs are that: MIL-53(Fe) has a characteristic wide peak of –OH between 3400 cm^{-1} and 3500 cm^{-1}, but there of NH_2-MIL-53(Fe) splits into two weak peaks, which are asymmetric stretching vibration (ν_{as}, ~3500 cm^{-1}) and symmetric stretching vibration (ν_s, ~3300 cm^{-1}) corresponding to *N*–H bond, respectively [36]. The two weak peaks together with the *C*–N bond near 1250 cm^{-1} confirm the presence of $-NH_2$ [37]. To sum up, NH_2-MIL-53(Fe) is a MOF formed by the coordination of Fe^{3+} and O of –COOH. As seen in Fig. 1C and Figs. S1B–C, the prepared NH_2-MIL-53(Fe) is fusiform, which with a diameter of about 300 nm along the long axis and about 200 nm along the short axis. On the other hand, MIL-53(Fe) has a rod-like structure with a size significantly larger than that of NH_2-MIL-53(Fe). And the average length of the rod is about 1.5 μM. The XPS analysis of NH_2-MIL-53(Fe) was performed and the survy spectrum is shown in Fig. 2A. In the Fe 2p spectrum (Fig. 2B), the binding energies at 711.8 eV and 725.4 eV are contributed to Fe $2p_{1/2}$ and Fe $2p_{3/2}$, respectively. And the doublet separation is 13.6 eV, which indicates the presence of Fe^{3+} [34,38]. The O 1s signal of NH_2-MIL-53(Fe) (Fig. 2C) at 531.7 eV and 532.5 eV is ascribable to Fe–O and carboxylate groups, respectively [34,39,40]. The N 1s peak (Fig. 2D) can be fitted to two components centered at 399.3 eV and 400.3 eV, which belong to *C*–N bond and NH_2 groups, respectively [34,39]. In the C 1s spectrum (Fig. 2E), by deconvolution, the phenyl bond, *C*–N bond and C=O bond are at 284.8 eV, 285.8 eV and 288.7 eV [34,41]. The XPS results further provide evidence for the successful introduction of amino groups into the MIL-53(Fe). All the data of characterization above are mainly uniform with the reported literature [34], so that we can go on the next research.

3.2. Electrochemical synergistic effect between HRP and NH_2- MIL-53(Fe)

Fig. S2A and B show the SEM and TEM characterization of the hybrid of NH_2-MIL-53(Fe) and HRP after storing in PBS (0.1 M, pH = 7.0) for 15 days. Compare Fig. 1C with Fig. S2A, the fusiform morphology and the size of NH_2-MIL-53(Fe) have not changed significantly. But after adding HRP, HRP will be adsorbed on the surface of NH_2-MIL-53(Fe) due to electrostatic adsorption. In the early stage of exploration, many attempts were made to promote the electron transfer between HRP and the surface of the electrode. Finally, we found that MWCNTs were favorable for improving the rate of electron transfer, but the peak is not obvious as shown in Fig. 3B. Then, when the mixture of NH_2-MIL-53(Fe) and HRP was modified on a semi-dry GCE coated with MWCNTs, the current response of NH_2-MIL-53(Fe)/HRP/MWCNTs/GCE was approximately twice as strong as the CV current response of the original HRP/MWCNTs/GCE in a 0.1 M PBS with a pH of 7.0, which is shown in Fig. 3C. This indicates that the Fe^{3+} ions of NH_2-MIL-53(Fe) has a good synergistic effect with the electrochemical active center Fe (III)/Fe (II) of HRP. In the early stage of research (Fig. 3D), with the addition of H_2O_2, the oxidation peak of the electrode gradually

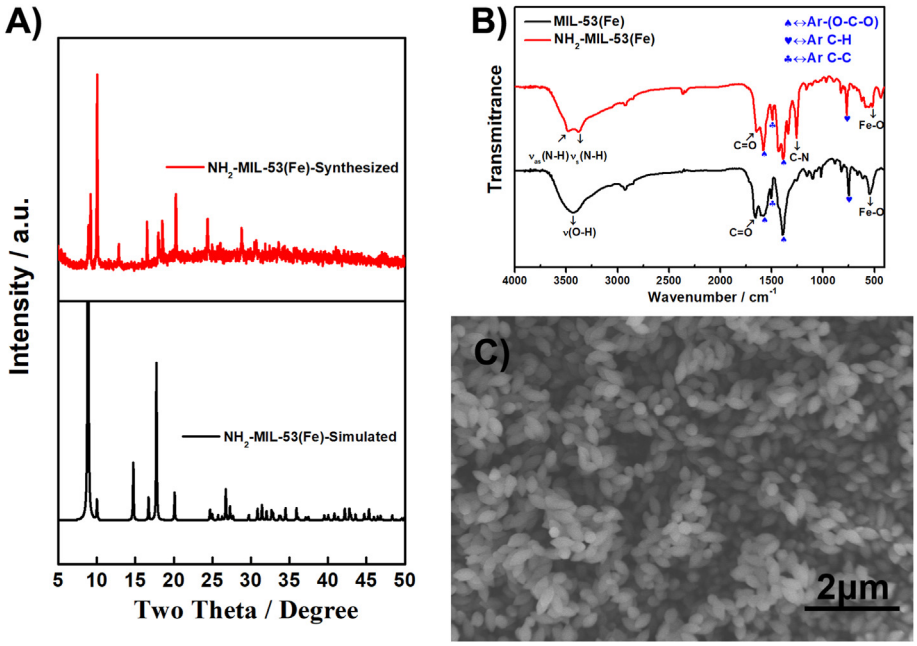

Fig. 1. (A) XRD patterns of NH_2-MIL-53(Fe); (**B**) FT-IR spectra; (**C**) SEM image of NH_2-MIL-53(Fe).

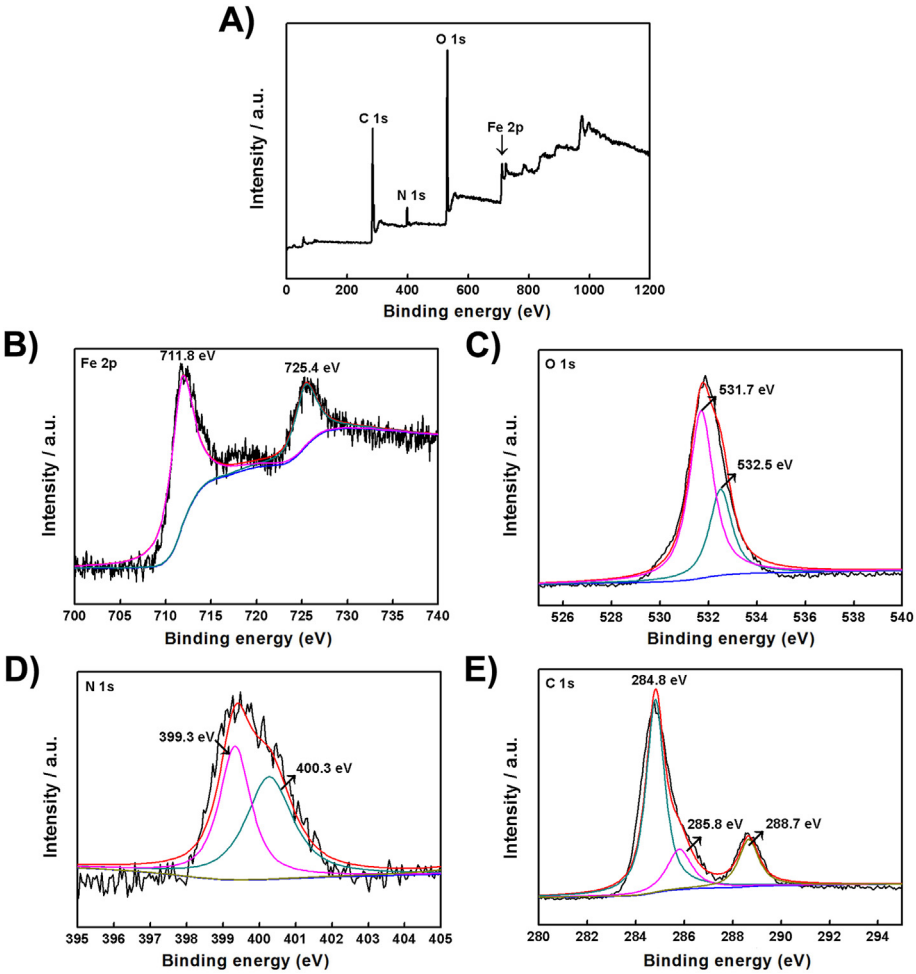

Fig. 2. A) XPS survey spectrum of NH_2-MIL-53(Fe). High-resolution XPS spectra of (**B**) Fe 2p, (**C**) O 1s, (**D**) N 1s and (**E**) C 1s.

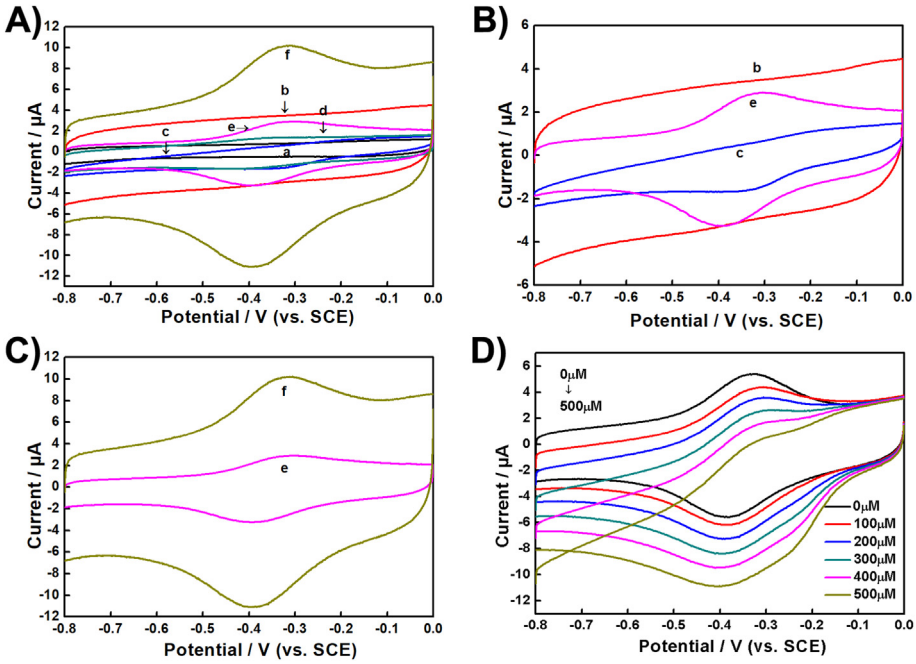

Fig. 3. (A-C) Cyclic voltammograms of the (a) GCE, (b) MWCNTs/GCE, (c) HRP/GCE, (d) NH_2-MIL-53(Fe)/GCE, (e) HRP/MWCNTs/GCE and (f) NH_2-MIL-53(Fe)/HRP/MWCNTs/GCE in 0.1 M PBS (pH = 7.0) at a scan rate of 150 mV/s. (**D**) CV curves of the NH_2-MIL-53(Fe)/HRP/MWCNTs/GCE in 0.1 M PBS buffer solution (pH = 7.0) with different concentrations of H_2O_2 at a scan rate of 100 mV/s.

decreased, while the reduction peak gradually increased, indicating that NH_2-MIL-53(Fe)/HRP/MWCNTs/GCE has good electrocatalytic performance for H_2O_2.

Electrochemical impedance spectroscopy (EIS) can be used to characterize the resistance of different electrodes. As illustrated in Fig. 4A, we study EIS of different modified electrodes in 2.5 mM $K_3Fe(CN)_6/K_4Fe(CN)_6$ solution containing 0.1 M KCl. Specific setting of relevant parameters was as follows: the initial potential was the open circuit potential, the frequency range was 0.01 Hz–100000 Hz, the ac amplitude is 0.005 V and the mode was single frequency. Fig. 4B–D shows electrodes modified by HRP, NH_2-MIL-53(Fe), NH_2-MIL-53(Fe)/HRP in the absence and presence of MWCNTs as carriers, it can be seen that the charge transfer resistance is greatly reduced due to the addition of MWCNTs, indicating that the MWCNTs material with good electrical conductivity can significantly enhance the electron transfer capacity of the electrode surface. Compare Fig. 4B and E, although the charge transfer resistance of HRP in potassium ferricyanide solution has been decreased by the addition of MWCNTs in a certain extent, then the addition of NH_2-MIL-53(Fe) can further reduce the electron transfer resistance. The result can be consistent with the cyclic voltammograms (CV), namely the CV current response of the direct electron transfer of NH_2-MIL-53(Fe)/HRP/MWCNTs/GCE is obvious higher than that of HRP/MWCNTs/GCE. Thus, the addition of NH_2-MIL-53(Fe) has significance in promoting HRP direct electrochemical current response. As evident in Fig. 4F, the charge transfer resistance of NH_2-MIL-53(Fe) is smaller than that of MIL-53(Fe), indicating the necessity of using terephthalic acid with amino group as the ligand for preparing the MOF in this experiment.

As illustrated in Figs. S3A and B, we investigate the effect of scan rate on the response of NH_2-MIL-53(Fe)/HRP/MWCNTs/GCE. We can find that both anodic and cathodic peak currents increase linearly with the scan rate, which implies that the electrode reaction is a surface adsorption-controlled redox process. As shown in Figs. S3C and D, the apparent formal peak potential has a linear relationship with pH from pH 5.0 to 9.0 with a slope of −50.25 mV/pH. This slope is close to the theoretical value for a reversible, one proton coupled with one-electron redox reaction process at 298.15 K [42].

3.3. The optimization of experimental conditions

Herein, we discuss the optimization of the experimental conditions, including the shaking time of NH_2-MIL-53(Fe)/HRP stock solution (Fig. S4), drying temperature of the modified electrodes (Fig. 5), the mass concentration ratio of HRP and MOF (Fig. S5), modification amount of the mixture of the MOF and the enzyme (Fig. S6), modification amount of MWCNTs (Fig. S7), the pH and the variety of buffer solution (Fig. S8) and the applied potential of i-t (Fig. 6A). More details can be seen in the supporting information.

A series of optimizations were made for the drying temperature of the electrodes here: 4, 20, 37, 50, 60 and 70 °C. As shown in Fig. 5, the peak shape measured by CV is symmetrical and the current can reach a high level at 37, 50 and 60 °C. Considering the possibility of damage to the electrode due to excessive temperature, 37 °C is finally selected as the optimal drying temperature.

We can observe from the data in Fig. 6A that the current response difference of NH_2-MIL-53(Fe)/HRP/MWCNTs/GCE toward the blank and 100 μM H_2O_2 is the largest at −0.40 V, so −0.40 V is selected as the best i-t applied potential. Moreover, Fig. 6B indicates that the addition of NH_2-MIL-53(Fe) has a good synergistic effect on the detection of H_2O_2 as well.

3.4. Electrochemical performance of NH_2-MIL-53(Fe)/HRP/MWCNTs/GCE toward H_2O_2

The analytical performance of NH_2-MIL-53(Fe)/HRP/MWCNTs/GCE toward H_2O_2 were studied by i-t technique at a potential of −0.40 V. Fig. 7 shows the i-t responses and the corresponding calibration curves for the electrochemical biosensor toward H_2O_2. As shown in Fig. 7B, D and F, the biosensor indicates two linear dynamic ranges of 0.1–1 μM ($I = -0.4313C - 0.1875$, $R^2 = 0.9974$) and 1–600 μM ($I = -0.01132C - 0.7441$, $R^2 = 0.9921$). The limit of

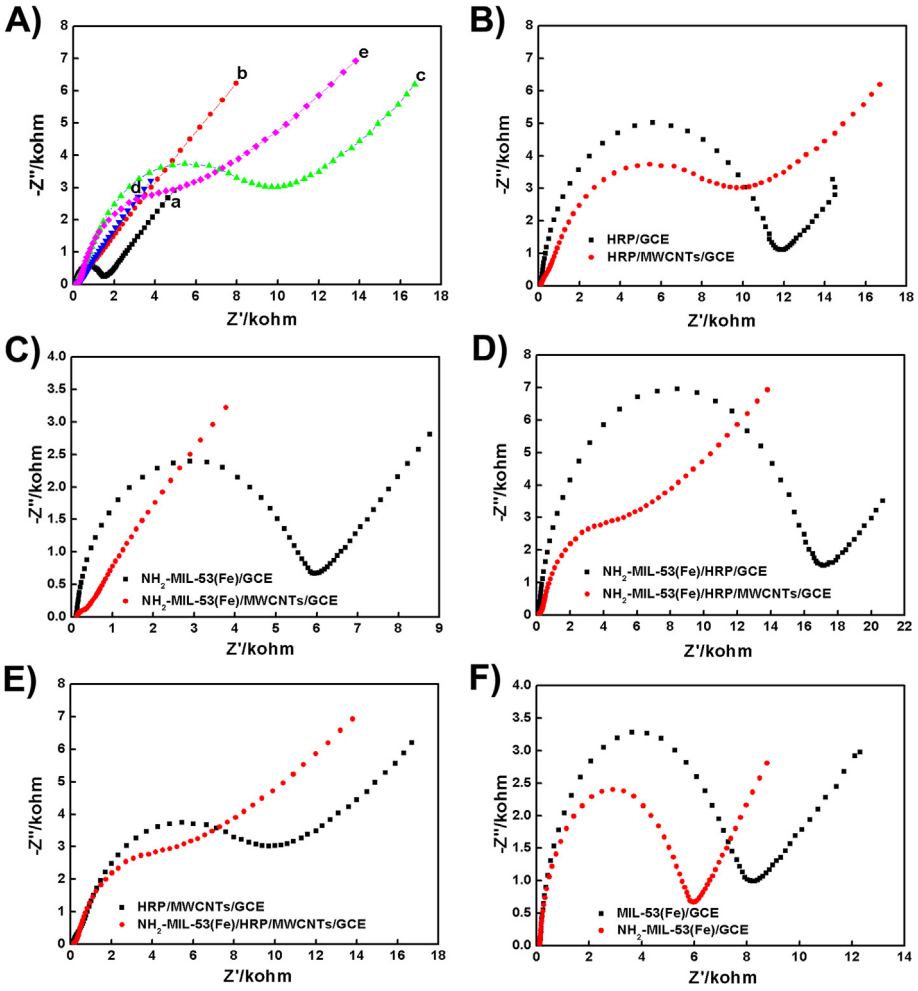

Fig. 4. (A) EIS of the (a) GCE, (b) MWCNTs/GCE, (c) HRP/MWCNTs/GCE, (d) NH_2-MIL-53(Fe)/MWCNTs/GCE and (e) NH_2-MIL-53(Fe)/HRP/MWCNTs/GCE in 2.5 mM $K_3Fe(CN)_6$/$K_4Fe(CN)_6$ solution containing 0.1 M KCl at open circuit voltage. (B-D) Nyquist plots of different modified electrodes with MWCNTs or not. (E) Nyquist plots of different modified electrodes with NH_2-MIL-53(Fe) or not. (F) Nyquist plots of electrodes modified by different MOFs with $-NH_2$ or not.

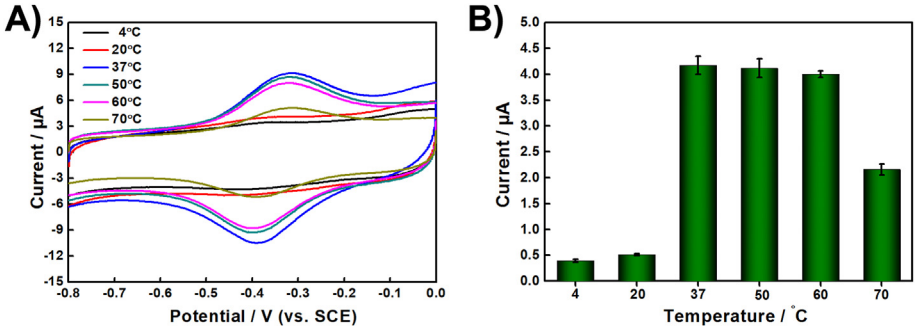

Fig. 5. (A) CV curves and (B) The bar graph of NH_2-MIL-53(Fe)/HRP/MWCNTs/GCE in 0.1 M PBS (pH = 7.0) at different drying temperatures of electrodes:4, 20, 37, 50, 60 and 70 °C. (Scan rate of CV curves: 100 mV/s)

detection (LOD) is estimated to be 0.028 μM (signal to noise ratio, S/N = 3). Comparison of analytical performance of NH_2-MIL-53(Fe)/HRP/MWCNTs/GCE with the other electrochemical biosensors is summarized in Table 1. The electrochemical biosensor reported in this work shows a low detection and high sensitivity.

To investigate the affinity between the immobilized HRP with H_2O_2, we used i-t method and Lineweaver–Burk equation $1/I_{ss}=(K_M/I_{max})(1/C)+(1/I_{max})$ [52] to calculate the apparent Michaelis–Menten constant (K_M) of immobilized HRP. Herein, I_{ss} is the steady-state current after the addition of substrate, C is the bulk concentration of the substrate and I_{max} is the maximum current measured under saturated substrate conditions. The K_M value was obtained by analysis of the slope and intercept for the linear calibration equation of I_{ss}^{-1} vs. C^{-1} (Fig. S14). The K_M value of the developed electrochemical sensor is 0.22 mM, which is much smaller than majority of the HRP-based electrodes (Table S3). The smaller K_M value suggests that HRP

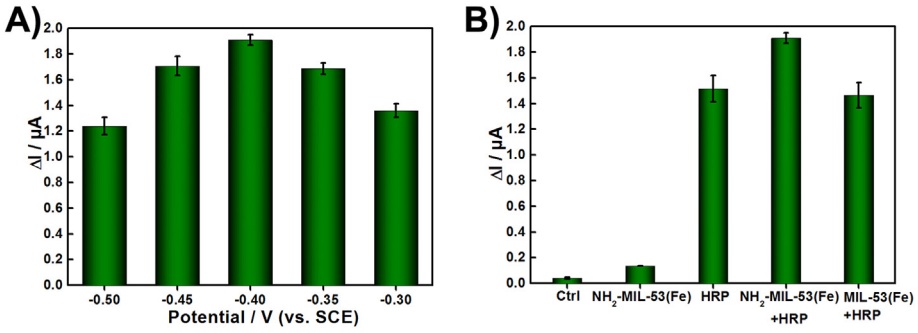

Fig. 6. The bar graph of i-t current responses to the difference of blank and 100 μM H_2O_2 (A) with different applied voltages and (B) different modified materials (Ctrl: only modifying 3 μL 1 mg/mL MWCNTs, the applied voltage is −0.4 V vs. SCE.).

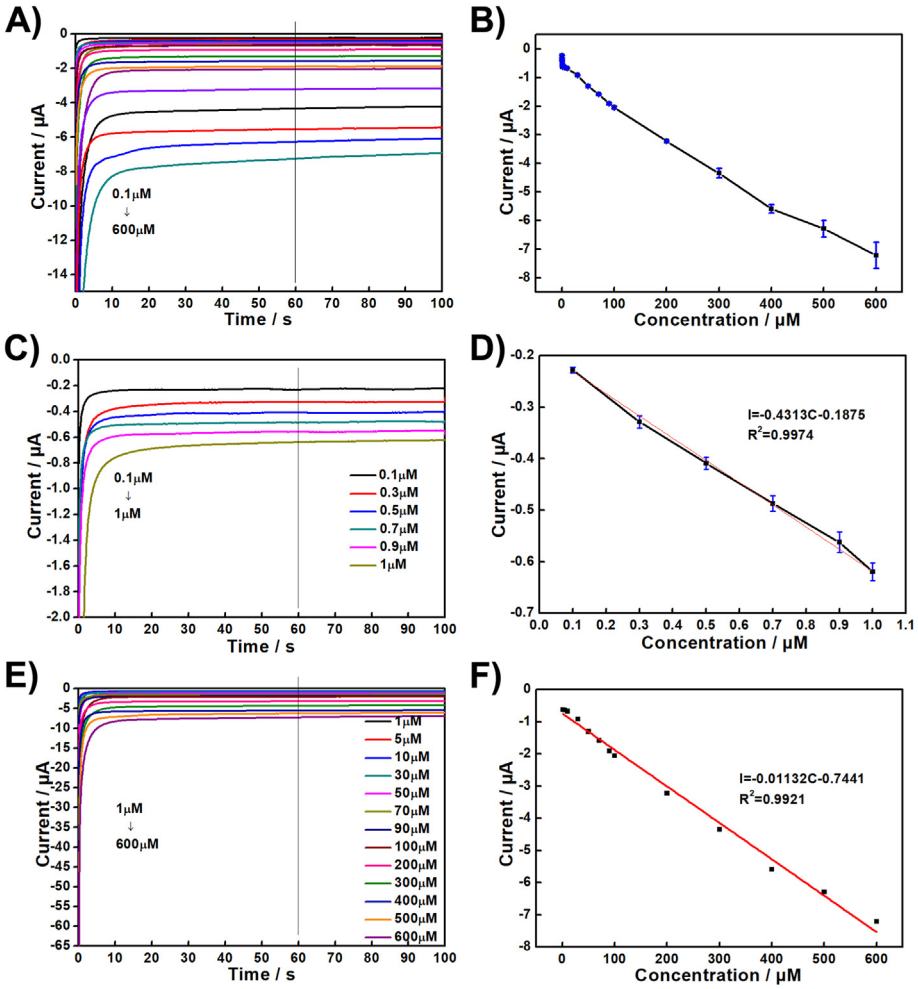

Fig. 7. The i-t response of NH2-MIL-53(Fe)/HRP/MWCNTs/GCE to different concentrations of H2O2 (A) from 0.1 μM to 600 μM, (C) from 0.1 μM to 1 μM, (E) from 1 μM to 600 μM. (B), (D) and (F) The corresponding calibration curve of I–C obtained by i-t to (A), (C) and (E), respectively.

immobilized on the NH_2-MIL-53(Fe) presents higher affinity. We can suppose from the result that NH_2-MIL-53(Fe) provides a better microenvironment for HRP immobilization, so it brings a synergistic electrocatalytical effect on H_2O_2. Moreover, as detailed in Figs. S15 and S16, the average peroxidase activity retention value of HRP immobilized on the electrodes obtained by TMB method is calculated as 60.59%, which indicates that the immobilized HRP can maintain certain peroxidase activity even after electrode drying at 37 °C for a long time.

3.5. Selectivity of NH_2-MIL-53(Fe)/HRP/MWCNTs/GCE

Selectivity or anti-interference ability is one of the important performances of electrochemical sensors. We selected many interfering substances, which are common in human body or cell cultivation solutions, including glucose, L-Ascorbic acid (AA), dopamine (DA), uric acid (UA), L-Lysine (Lys), L-Glycine (Gly), L-Glutamic acid (Glu) and L-aspartic acid (Asp). After the blank current is stabilized, adding 100 μM H_2O_2 and the current change is relatively obvious (Fig. 8A).

Table 1
Comparison of analytical performance of NH_2-MIL-53(Fe)/HRP/MWCNTs/GCE with other electrochemical biosensors.

Working electrode	Methods	Linear range (μM)	LOD (μM)	Sensitivity (μA mM^{-1} cm^{-2})	References
Taurine-functionalized graphene foam	CV	0.5–300, 2000-10000	0.1	NR	[43]
3D rGO foam-hemin/GCE	DPV	0.005–5000	0.003	50.5	[44]
CMC@Pd/Al-LDH/GCE	DPV	1–120	0.3	16.27	[45]
HRP/C-Dots/LDHs/GCE	i-t	0.1–23.1	0.04	470	[46]
Mg_3Fe-Hb/GC	i-t	0.07–2.51	0.036	390.66	[47]
MIL-53-Cr^{III}_{AS}/GCE	DPV	25–500	~3.52	168.44	[48]
MIL-100(Fe)@LMC/GCE	i-t	1–5000	1.2	298	[49]
Cu MOF/SPE	i-t	10-1000, 1400-6800	4.1	NR	[50]
Zn-MOF/rGO/CPE	i-t	1–625	0.05	4.01	[51]
NH_2-MIL-53(Fe)/HRP/MWCNTs/GCE	i-t	0.1–1, 1-600	0.028	6149.2, 155.74	This work

Then adding different kinds of interfering substances (1 mM) every 50 s, we can easily find that all the interfering substances with 10 times of H_2O_2 concentration has no significant impact on the i-t stabilized current. However, when we changed another way, which was as same as how to obtain the calibration curves, to study the anti-interference ability (Fig. 8B), we can find that AA has a larger influence on the control experiment. Thus, when the buffer solution contains 100 μM H_2O_2 and 1 mM AA simultaneously, the completely stable i-t current response is 17.24% lower than that of only 100 μM H_2O_2. The main reason may be that AA has strong reducibility, a large amount of AA can accelerate the reduction of H_2O_2 as time goes on. To sum up, the interference of 10 times H_2O_2 concentration of interfering substances is within a controllable range, and the overall anti-interference ability of the electrode is good.

3.6. Reproducibility of NH_2-MIL-53(Fe)/HRP/MWCNTs/GCE

The reproducibility of NH_2-MIL-53(Fe)/HRP/MWCNTs/GCE to blank, 100 μM H_2O_2 and the difference between 100 μM H_2O_2 and blank responses were investigated by means of the parallel modification of five GCEs. As shown in Fig. S12, the relative standard deviation (RSD) of the i-t current value of the blank of the five electrodes is 6.62%, the RSD of the i-t current value of 100 μM H_2O_2 is 2.16%, and the RSD of the i-t current difference between the blank and 100 μM H_2O_2 is 2.13%. Note that each data here is plotted with the absolute value of the original data. In general, the electrochemical biosensor has great reproducibility.

3.7. Stability of NH_2-MIL-53(Fe)/HRP and NH_2-MIL-53(Fe)/HRP/MWCNTs/GCE biosensor

Stability experiment is divided into two parts: one is the stability of the modified material itself; another is the stability of the electrochemical biosensor sensing performance. Combine SEM, XRD and UV–vis data as shown in Figs. S10–S12, we can find that NH_2-MIL-53(Fe) has good water stability for about a week, but long-term storage has a great impact on the stability of HRP. So NH_2-MIL-53(Fe)/HRP stock solution had better be used within a week, otherwise it will affect the performance of the sensor.

To investigate the stability of the sensing performance of the electrochemical biosensor, two NH_2-MIL-53(Fe)/HRP/MWCNTs/GCEs were modified in parallel, one in the refrigerator (approx. 4 °C) and one at room temperature (approx. 15 °C). The i-t current response difference between the blank and 100 μM H_2O_2 in 18 days of cold storage and room temperature storage (ΔI is 100% on the day of electrode preparation) is recorded in Figs. S13A and B, respectively. The results show that cold storage is not optimistic for the stability of electrode sensing performance, and ΔI is reduced to 57.80% at 18 days. Meanwhile, the stability of the electrode sensing performance stored at room temperature is better than that stored at 4 °C, it maintains more than 90% of the original within a week and more than 70% of the original on the 18th day.

In conclusion, NH_2-MIL-53(Fe)/HRP material can maintain water stability for about a week, and the sensing performance of NH_2-MIL-53(Fe)/HRP/MWCNTs/GCE at room temperature (approx. 15 °C) can reach more than 90% stability within a week, and gradually decrease to less than 80% after two weeks. Overall, this electrochemical biosensor has good stability.

3.8. Real samples analysis

The complete medium used in cell culture and the culture medium of the two types of cancer cells collected during cell passage were divided into three centrifuge tubes. After the blank current of PBS (pH = 7.0, 5 mL) was measured by the NH_2-MIL-53(Fe)/HRP/MWCNTs/GCE, 10 μL complete medium was transferred with a micro

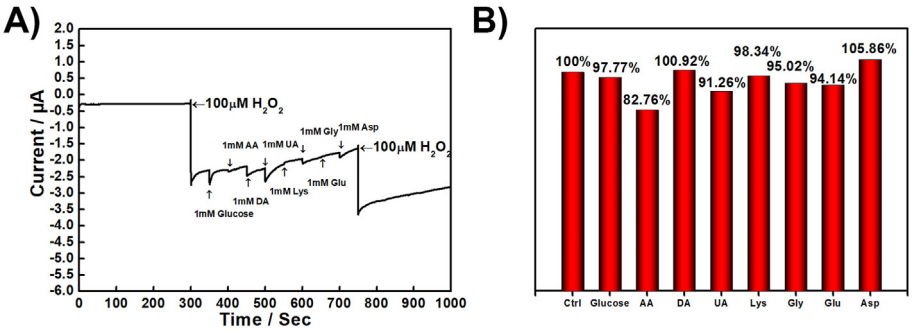

Fig. 8. (A) The amperometric response of the NH_2-MIL-53(Fe)/HRP/MWCNTs/GCE to 1 mM different interfering substances such as Glucose, AA, DA, UA, L-Lysine (Lys), L-Glycine (Gly), L-Glutamic acid (Glu) and L-Aspartic acid (Asp) (The concentration of H_2O_2 is 100 μM, the applied voltage is -0.4 V vs. SCE). (**B**) The bar graph of i-t current responses to the difference of blank and 100 μM H_2O_2 with 1 mM different interfering substances in 0.1 M PBS (pH = 7.0). (Ctrl = Control, which represents the i-t response difference of blank and 100 μM H_2O_2.)

Table 2
Concentration comparison of H_2O_2 released from cancer cells treated with ART or not.

Cell culture solutions	Control μM	ART-treated μM
Hela	36.14 ± 3.42	43.50 ± 5.28
HepG2	55.17 ± 4.59	62.36 ± 6.03

syringe and added to the buffer solution above. Experimental data were recorded when the current values obtained by i-t method were stable, we found that the current values ware almost unchanged from the original blank current, indicating that there was no H_2O_2 in the complete medium without cell culture (data not shown). The response current values of NH_2-MIL-53(Fe)/HRP/MWCNTs/GCEs to HeLa cell and HepG2 cell cultivation solutions were recorded using the same experimental method, the concentration of H_2O_2 in the electrolytic cell solution was obtained by comparing the average value of the three parallel measurements with the linear relationship between i-t current and H_2O_2 concentration. When we multiplied the concentrations obtained above by the diluted multiple, we could finally get the actual concentrations of H_2O_2 in the original cultivation solutions collected. The actual H_2O_2 concentrations of the two samples are calculated in Table S4. In order to verify the accuracy of this electrochemical sensor, we used the detection results of the UV–vis method (detailed in the supporting information) as the control. The results of the two methods are not significantly different, indicating that the electrochemical sensor can be successfully used to directly detect the concentration of H_2O_2 released by cancer cells.

Evidence is accumulating that extracellular environments comprising growth factors and cytokines operate through complex intracellular signal transduction networks that ultimately control cellular fates [53]. Responses of cells to extracellular environments are implicated in cell survival, proliferation, differentiation, and death to progress normal development and maintain tissue homeostasis in multicellular organisms [54]. Artemisinin (ART) and its derivatives are considered as promising drugs for the treatment of cancer, and their main action seems to be directed toward stalling tumor cell proliferation through cell cycle arrest mediated by reactive oxygen species (ROS) [55]. By comparing H_2O_2 generated from cells along with the cell environment changing caused by the co-culture of 100 μM ART (Table 2), we can know whether the proliferation of cancer cells is inhibited by anticancer drugs. According to literature [56–58], the addition of ART-related drugs can induce the production of ROS, so the H_2O_2 concentration in the cell culture solution treated with ART is higher. Our experimental data are consistent with the literature reported before, so our electrochemical sensor has certain practical application value.

4. Conclusions

The electrochemical biosensor presented in the work was prepared by simply using untreated MWCNTs as conductive carrier, which could maintain its structure and properties to the maximum extent. Then, the electrode through a simple physical mixing method to combine NH_2-MIL-53(Fe) with HRP and showed a good synergistic effect between the Fe (III)/Fe (II) redox active center. In the supporting information, we detailed the conditional optimization to obtain an electrochemical sensor with excellent rate of electron transfer. And the analytical performance of the biosensor was satisfactory due to its low detection limit, high sensitivity and good stability. In addition, the stability of NH_2-MIL-53(Fe) and HRP were discussed by three methods. To get a reliable performance of the electrochemical biosensor, considering the short-term water stability of materials, the stock solutions were supposed to be used in a week. This work also developed a new platform for direct detection of H_2O_2 released by cancer cells and has been demonstrated to be meaningful for monitoring the change of cell generated H_2O_2 along with the cell environment changing.

CRediT authorship contribution statement

Tian Jiang: Investigation, Writing - original draft. **Xiuxiu Sun:** Investigation, Visualization. **Lingli Wei:** Formal analysis. **Maoguo Li:** Conceptualization, Writing - review & editing, Supervision.

Declaration of competing interest

The authors declare that they have no known competing financial interests or personal relationships that could have appeared to influence the work reported in this paper.

Acknowledgements

We thank the National Natural Science Foundation of China (21075001) for support of this research. This work is also supported by Foundation for Innovation Team of Bioanalytical Chemistry. Ms. L.L. Wei thanks the Chinese University Student Innovation Training Programs (201910370039) for financial support.

Appendix A. Supplementary data

Supplementary data to this article can be found online at https://doi.org/10.1016/j.aca.2020.09.040.

References

[1] C.-Y. Wang, S.-M. Huang, L.-Z. Luo, Y. Zhou, X.-C. Lu, G. Zhang, H. Ye, J.-J. Gu, F.-F. Cao, Ultrathin two-dimension metal-organic framework nanosheets/multi-walled carbon nanotube composite films for the electrochemical detection of H_2O_2, J. Electroanal. Chem. 835 (2019) 178–185.
[2] C.C. Wang, Y. Wang, G.Y. Wang, C.S. Huang, N.Q. Jia, A new mitochondria-targeting fluorescent probe for ratiometric detection of H_2O_2 in live cells, Anal. Chim. Acta 1079 (2020) 230–237.
[3] S.S. Mohammadi, Z. Vaezi, B. Shojaedin-Givi, H. Naderi-Manesh, Chemiluminescent liposomes as a theranostic carrier for detection of tumor cells under oxidative stress, Anal. Chim. Acta 1059 (2019) 113–123.
[4] J. St-Pierre, S. Drori, M. Uldry, J.-M. Silvaggi, J. Rhee, S. Jäger, C. Handschin, K.-N. Zheng, J.-D. Lin, W.-L. Yang, D.K. Simon, R. Bachoo, B.-M. Spiegelman, Suppression of reactive oxygen species and neurodegeneration by the PGC-1 transcriptional coactivators, Cell 127 (2006) 397–408.
[5] N. Yusoff, P. Rameshkumar, M.-S. Mehmood, A. Pandikumar, H.-W. Lee, N.-M. Huang, Ternary nanohybrid of reduced graphene oxide-Nafion@Silver nanoparticles for boosting the sensor performance in non-enzymatic amperometric detection of hydrogen peroxide, Biosens. Bioelectron. 87 (2017) 1020–1028.
[6] Y.M. Fu, D. Huang, C.M. Li, L.N. Zou, B.X. Ye, Graphene blended with SnO_2 and Pd-Pt nanocages for sensitive nonenzymatic electrochemical detection of H_2O_2 released from living cells, Anal. Chim. Acta 1014 (2018) 10–18.
[7] N. Gong, X. Ma, X. Ye, Q. Zhou, X. Chen, X. Tan, S. Yao, S. Huo, T. Zhang, S. Chen, X. Teng, X. Hu, J. Yu, Y. Gan, H. Jiang, J. Li, X. Liang, Carbon-dot-supported atomically dispersed gold as a mitochondrial oxidative stress amplifier for cancer treatment, Nat. Nanotechnol. 14 (2019) 379–387.
[8] N.-V. Klassen, D. Marchlngton, H.-C.-E. McGowan, H_2O_2 Determination by the I_3^- method and by $KMnO_4$ titration, Anal. Chem. 66 (1994) 2921–2925.
[9] M.-M. Liu, S.-H. Li, D.-D. Huang, Z.-W. Xu, Y.-W. Wu, Y. Lei, A.-L. Liu, MoO_x quantum dots with peroxidase-like activity on microfluidic paper-based analytical device for rapid colorimetric detection of H_2O_2 released from PC12 cells, Sensor, Actuat. B-Chem. 305 (2020) 127512.
[10] Z.Q. Zhou, L.Y. Yang, L. Huang, Y.P. Liao, Y. Liu, Q. Xiao, A novel fluorescent probe for H_2O_2 detection based on CdSe@ZnS quantum dots/Ag nanocluster hybrid, Anal. Chim. Acta 1106 (2020) 176–182.
[11] J. Liu, J.J. Liang, C.L. Wu, Y.B. Zhao, A doubly-quenched fluorescent probe for low-background detection of mitochondrial H_2O_2, Anal. Chem. 91 (2019) 6902–6909.
[12] Y.-L. Sun, Y.-N. Lin, W.-Y. Sun, R. Han, C.-N. Luo, X.-Y. Wang, Q. Wei, A highly selective and sensitive detection of insulin with chemiluminescence biosensor based on aptamer and oligonucleotide-AuNPs functionalized nanosilica@graphene oxide aerogel, Anal. Chim. Acta 1089 (2019) 152–164.

[13] F.-J. Chen, D. Wang, J. Chen, J.-J. Ling, H. Yue, L.-X. Gou, H. Tang, PtNi nanocubes-catalyzed tyramine signal amplification electrochemiluminescence sensor for nonenzymatic and ultrasensitive detection of hepatocellular carcinoma cells, Sensor. Actuator. B Chem. 305 (2020) 127472.
[14] J. Ju, X.J. Liu, J.J. Yu, K. Sun, F. Fathi, X.Q. Zeng, Electrochemistry at bimetallic Pd/Au thin film surfaces for selective detection of reactive oxygen species and reactive nitrogen species, Anal. Chem. 92 (2020) 6538–6547.
[15] S.H. Wu, X.B. Huang, Y. Tang, L.M. Ma, Y. Liu, J.J. Sun, Temperature controllable electrochemical sensors based on horseradish peroxidase as electrocatalyst at heated Au disk electrode and its preliminary application for H_2O_2 detection, Anal. Chim. Acta 1096 (2020) 44–52.
[16] Y.J. Sun, M.C. Luo, X.X. Meng, J. Xiang, L. Wang, Q.S. Ren, S.J. Guo, Graphene/intermetallic PtPb nanoplates composites for boosting electrochemical detection of H_2O_2 released from cells, Anal. Chem. 89 (2017) 3761–3767.
[17] L. Li, B.-Y. Li, H. Liu, M.-Q. Li, B.-H. Wang, Photoelectrochemical sensing of hydrogen peroxide using TiO_2 nanotube arrays decorated with RGO/CdS, J. Alloys Compd. 815 (2020) 152241.
[18] M. Shamsipur, M. Asgari, M.-F. Mousavi, R. Davarkhah, A novel hydrogen peroxide sensor based on the direct electron transfer of catalase immobilized on nano-sized NiO/MWCNTs composite film, Electroanalysis 24 (2012) 357–367.
[19] K. Yamamoto, G.-Y. Shi, T.-S. Zhou, F. Xu, J.-M. Xu, T. Kato, J.-Y. Jin, L.-T. Jin, Study of carbon nanotubes-HRP modified electrode and its application for novel on-line biosensors, Analyst 128 (2013) 249–254.
[20] J. Yang, W.-D. Zhang, S. Gunasekaran, A low-potential, H_2O_2-assisted electrodeposition of cobalt oxide/hydroxide nanostructures onto vertically-aligned multi-walled carbon nanotube arrays for glucose sensing, Electrochim. Acta 56 (2011) 5538–5544.
[21] A.-P. Periasamy, S.-Y. Yang, S.-M. Chen, Preparation and characterization of bismuth oxide nanoparticles-multiwalled carbon nanotube composite for the development of horseradish peroxidase based H_2O_2 biosensor, Talanta 87 (2011) 15–23.
[22] X.-Q. Liu, R. Yan, J.M. Zhang, J. Zhu, D.-K.-Y. Wong, Evaluation of a carbon nanotube-titanate nanotube nanocomposite as an electrochemical biosensor scaffold, Biosens. Bioelectron. 66 (2015) 208–215.
[23] W.-F. Dong, L.-D. Liu, W.-B. Shi, Y.-M. Huang, Metal-organic framework MIL-53(Fe): facile microwave-assisted synthesis and use as a highly active peroxidase mimetic for glucose biosensing, RSC Adv. 5 (2015) 17451.
[24] Y.-H. Li, X.-Y. You, X.-Y. Shi, Enhanced Chemiluminescence Determination of hydrogen peroxide in milk sample using metal-organic framework Fe-MIL-88NH_2 as peroxidase mimetic, Food Anal. Method. 10 (2017) 626–633.
[25] L.-Z. Yang, C.-L. Xu, W.-C. Ye, W.-S. Liu, An electrochemical sensor for H_2O_2 based on a new Co-metal-organic framework modified electrode, Sensor. Actuator. B Chem. 215 (2015) 489–496.
[26] D. Li, S. Zhang, X. Feng, H. Yang, F. Nie, W. Zhang, A novel peroxidase mimetic Co-MOF enhanced luminol chemiluminescence and its application in glucose sensing, Sensor. Actuator. B Chem. 296 (2019) 126631, https://doi.org/10.1016/j.snb.2019.126631.
[27] Y. Shu, J.-Y. Chen, Z. Xu, D.-Q. Jin, Q. Xu, X.-Y. Hu, Nickel metal-organic framework nanosheet/hemin composite as biomimetic peroxidase for electrocatalytic reduction of H_2O_2, J. Electroanal. Chem. 845 (2019) 137–143.
[28] J.-Y. Chen, Y. Shu, H.-L. Li, Q. Xu, X.-Y. Hu, Nickel metal-organic framework 2D nanosheets with enhanced peroxidase nanozyme activity for colorimetric detection of H_2O_2, Talanta 189 (2018) 254–261.
[29] S.-S. Menon, S.-V. Chandran, A. Koyappayil, S. Berchmans, Copper-based metal-organic frameworks as peroxidase mimics leading to sensitive H_2O_2 and glucose detection, Chemistry 3 (2018) 8319–8324.
[30] J.-Y. Wang, W.-Y. Li, Y.-Q. Zheng, Nitro-functionalized metal-organic frameworks with catalase mimic properties for glutathione detection, Analyst 144 (2019) 6041.
[31] M.-Y. Shi, M. Xu, Z.-Y. Gu, Copper-based two-dimensional metal-organic framework nanosheets as horseradish peroxidase mimics for glucose fluorescence sensing, Anal. Chim. Acta 1079 (2019) 164–170.
[32] H.-Q. Zheng, C.-Y. Liu, X.-Y. Zeng, J. Chen, J. Lü, R.-G. Lin, R. Cao, Z.-J. Lin, J.-W. Su, MOF-808: a metal-organic framework with intrinsic peroxidase-like catalytic activity at neutral pH for colorimetric biosensing, Inorg. Chem. 57 (2018) 9096–9104.
[33] C.-H. Wang, X.-L. Liu, N.-K. Demir, J.-P. Chen, K. Li, Applications of water stable metal-organic frameworks, Chem. Soc. Rev. 45 (2016) 5107–5134.
[34] X.-X. Zheng, L.-J. Shen, X.-P. Chen, X.-H. Zheng, C.-T. Au, L.-L. Jiang, Amino-modified Fe-terephthalate metal-organic framework as an efficient catalyst for the selective oxidation of H_2S, Inorg. Chem. 57 (2018) 10081–10089.
[35] Y. Jiang, Q.-M. Yang, Q.-J. Xu, S.-Y. Lu, L.-Y. Hu, M.-W. Xu, Y.-S. Liu, Metal organic framework MIL-53(Fe) as an efficient artificial oxidase for colorimetric detection of cellular biothiols, Anal. Biochem. 577 (2019) 82–88.
[36] T. Devic, P. Horcajada, C. Serre, F. Salles, G. Maurin, B. Moulin, D. Heurtaux, G. Clet, A. Vimont, J.-M. Grenèche, B.L. Ouay, F. Moreau, E. Magnier, Y. Filinchuk, J. Marrot, J.-C. Lavalley, M. Daturi, G. Férey, Functionalization in flexible porous solids: effects on the pore opening and the host-guest interactions, J. Am. Chem. Soc. 132 (2010) 1127–1136.
[37] L. Shen, S. Liang, W. Wu, R. Liang, L. Wu, Multifunctional NH_2-mediated Zirconium metal-organic framework as an efficient visible-light-driven photocatalyst for selective oxidation of alcohols and reduction of aqueous Cr(VI), Dalton Trans. 42 (2013) 13649.
[38] H.P. Uppara, H. Dasari, S.K. Singh, N.K. Labhsetwar, M.S. Murari, Effect of copper doping over $GdFeO_3$ perovskite on soot oxidation activity, Catal. Lett. 149 (2019) 3097–3110.
[39] H. Guo, D. Wang, J. Chen, W. Weng, M. Huang, Z. Zheng, Simple fabrication of flake-like NH_2-MIL-53(Cr) and its application as an electrochemical sensor for the detection of Pb^{2+}, Chem. Eng. J. 289 (2016) 479–485.
[40] E.V. Ramos-Fernandez, C. Pieters, B. Linden, J. Juan-Alcañiz, P. Serra-Crespo, M.W.G.M. Verhoeven, H. Niemantsverdriet, J. Gascon, F. Kapteijn, Highly dispersed platinum in metal organic framework NH_2-MIL-101(Al) containing phosphotungstic acid-characterization and catalytic performance, J. Catal. 289 (2012) 42–52.
[41] T.A. Vu, G.H. Le, C.D. Dao, L.Q. Dang, K.T. Nguyen, Q.K. Nguyen, P.T. Dang, H.T.K. Tran, Q.T. Duong, T.V. Nguyen, G.D. Lee, Arsenic removal from aqueous solutions by adsorption using novel MIL-53(Fe) as a highly efficient adsorbent, RSC Adv. 5 (2015) 5261–5268.
[42] F.-H. Wu, J.-J. Xu, Y. Tian, Z.-C. Hu, L.-W. Wang, Y.-Z. Xian, L.-T. Jin, Direct electrochemistry of horseradish peroxidase on TiO_2 nanotube arrays via seeded-growth synthesis, Biosens. Bioelectron. 24 (2008) 198–203.
[43] Z.-Y. Guo, Y.-F. Feng, Y.-Y. Chen, Q.-H. Yao, H.-Z. Luo, X. Chen, A taurine-functionalized 3D graphene-based foam for electrochemical determination of hydrogen peroxide, Talanta 208 (2020) 120356, https://doi.org/10.1016/j.talanta.2019.120356.
[44] Q. Li, Y. Zhang, P. Li, H. Xue, N. Jia, A nanocomposite prepared from hemin and reduced graphene oxide foam for voltammetric sensing of hydrogen peroxide, Microchim. Acta 187 (2020) 45, https://doi.org/10.1007/s00604-019-3829-3.
[45] G. Fazli, S.-E. Bahabadi, L. Adlnasab, H. Ahmar, A glassy carbon electrode modified with a nanocomposite prepared from Pd/Al layered double hydroxide and carboxymethyl cellulose for voltammetric sensing of hydrogen peroxide, Microchim. Acta 186 (2019) 821, https://doi.org/10.1007/s00604-019-3967-7.
[46] Y.-L. Wang, Z.-C. Wang, Y.-P. Rui, M.-G. Li, Horseradish peroxidase immobilization on carbon nanodots/CoFe layered double hydroxides: direct electrochemistry and hydrogen peroxide sensing, Biosens. Bioelectron. 64 (2015) 57–62.
[47] M.-G. Li, H.-Q. Ji, Y.-L. Wang, L. Liu, F. Gao, MgFe-layered double hydroxide modified electrodes for direct electron transfer of heme proteins, Biosens. Bioelectron. 38 (2012) 239–244.
[48] N.-S. Lopa, M.-M. Rahman, F. Ahmed, S.-C. Sutradhar, A base-stable metal-organic framework for sensitive and non-enzymatic electrochemical detection of hydrogen peroxide, Electrochim. Acta 274 (2018) 49–56.
[49] J.-Y. Lin, M. Hassan, X.-J. Bo, L.-P. Guo, Synthesis of iron-based metal-organic framework@large mesoporous carbon composites and their electrocatalytic properties, J. Electroanal. Chem. 801 (2017) 373–380.
[50] W. Ling, Y.-F. Hao, H.-J. Wang, H. Xu, X. Huang, A novel Cu-metal-organic framework with two-dimensional layered topology for electrochemical detection using flexible sensors, Nanotechnology 30 (2019) 42, https://doi.org/10.1088/1361-6528/ab30b6.
[51] S.-L. Yang, N. Xia, M.-Y. Li, P.-P. Liu, Y.-X. Wang, L.-B. Qu, Facile synthesis of a zeolitic imidazolate framework-8 with reduced graphene oxide hybrid material as an efficient electrocatalyst for nonenzymatic H_2O_2 sensing, RSC Adv. 9 (2019) 15217–15223.
[52] R.A. Kamin, G.S. Wilson, Rotating ring-disk enzyme electrode for biocatalysis kinetic studies and characterization of the immobilized enzyme layer, Anal. Chem. 52 (1980) 1198–1205.
[53] K.A. Janes, J.G. Albeck, S. Gaudet, P.K. Sorger, D.A. Lauffenburger, M.B. Yaffe, A systems model of signaling identifies a molecular basis set for cytokine-induced apoptosis, Science 310 (2005) 1646–1653.
[54] K.A. Janes, J.G. Albeck, S. Gaudet, P.K. Sorger, D.A. Lauffenburger, M.B. Yaffe, A systems model of signaling identifies a molecular basis set for cytokine-induced apoptosis, Science 310 (2005) 1646–1653.
[55] A. Bhaw-Luximon, D. Jhurry, Artemisinin and its derivatives in cancer therapy: status of progress, mechanism of action, and future perspectives, Canc. Chemother. Pharmacol. 79 (2017) 451–466.
[56] J.G. Jia, Y.Y. Qin, L.G. Zhang, C.X. Guo, Y.G. Wang, X.C. Yue, J. Qian, Artemisinin inhibits gallbladder cancer cell lines through triggering cell cycle arrest and apoptosis, Mol. Med. Rep. 13 (2016) 4461–4468.
[57] A. Zyad, M. Tilaoui, A. Jaafari, M.A. Oukerrou, H.A. Mouse, More insights into the pharmacological effects of artemisinin, Phytother Res. 32 (2017) 216–229.
[58] I. Tsamesidis, P. Pério, A. Pantaleo, K. Reybier, Oxidation of erythrocytes enhance the production of reactive species in the presence of artemisinins, Int. J. Mol. Sci. 21 (2020) 4799.